Minimum-dissipation principle for synchronised stochastic oscillators far from equilibrium

Jan Meibohm^{1,2} and Massimiliano Esposito³

¹Technische Universität Berlin, Straße des 17. Juni 135, 10623 Berlin, Germany
 ²Department of Mathematics, King's College London, London WC2R 2LS, United Kingdom
 ³Complex Systems and Statistical Mechanics, Department of Physics and Materials Science, University of Luxembourg, L-1511 Luxembourg, Luxembourg

We prove a linear stability-dissipation relation (SDR) for q-state Potts models driven far from equilibrium by a nonconservative force. At a critical coupling strength, these models exhibit a synchronisation transition from a decoherent into a synchronised state. In the vicinity of this transition, the SDR connects the entropy production rate per oscillator to the phase-space contraction rate, a measure of stability, in a simple way. For large but finite systems, we argue that the SDR implies a minimum-dissipation principle for driven Potts models as the dynamics selects stable non-equilibrium states with least dissipation. This principle holds arbitrarily far from equilibrium, for any stochastic dynamics, and for all q.

INTRODUCTION

Both equilibrium and non-equilibrium systems may exhibit order, characterised by spontaneously broken symmetries, long-range correlations, and macroscopic structure. At equilibrium, order is strictly constrained by the laws of thermodynamics, which force it to be stable and static. By contrast, far from equilibrium, where fluctuations prevail, irreversible dynamic processes lead to the appearance of so-called dissipative structures [1, 2], that may occur in a much richer variety of both stationary and dynamic patterns.

The theory of dissipative structures is closely bound to irreversibility [1, 2] and to the dissipation of entropy [3–5]. For near-equilibrium steady states [6, 7], Prigogine's theorem [3] asserts that entropy production is minimal and constant [8]. However, no such general statements hold far from equilibrium, where counter examples are known [9–11]. Generalisations of minimum-dissipation principles à la Prigogine to far-from-equilibrium systems have been attempted by many, but are hindered by the phenomenological nature of conventional non-equilibrium extremum principles in the spirit of Gibbs' maximum entropy principle have fascinated statistical physicists for almost two centuries [12].

Stochastic Thermodynamics [13–15] governs mesoscopic scales where fluctuations are abundant. Within Stochastic Thermodynamics, interactions between the system and the environment are treated as random and are equipped with a consistent thermodynamic interpretation. Thermodynamic consistency then holds when a local detailed balance (LDB) condition is fulfilled [13–15]. Recent developments [16] allow the analysis of thermodynamically consistent, mesoscopic models in the thermodynamic limit, connecting Stochastic Thermodynamics with the classical theory of non-equilibrium thermodynamics. This connection provides previously phenomenological macroscopic laws of non-equilibrium thermodynamics with a consistent justification.

In this Letter, we employ this connection to shed new light on the old question of the existence of minimum-dissipation principles far from equilibrium. We analyse a family of

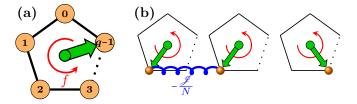


FIG. 1. (a) Potts spin (green arrow) with q states (orange bullets), driven by a non-conservative force f (red arrow). (b) The energy of interacting Potts spins is reduced by \mathcal{J}/N whenever two spins are aligned.

thermodynamically consistent oscillators, so-called driven q-state Potts models [17, 18], that consist of N globally interacting Potts spins. A Potts spin can be thought of as a two-dimensional unit vector, that points into one out of q equally-spaced directions, see Figure 1(a). We denote by s_m , $m = 1, \ldots, N$, the state of the mth Potts spin, which may take any integer value between 0 and q-1.

The states s_m change stochastically through a dynamics that models the interactions of the system with a heat bath at inverse temperature $\beta = 1/(k_BT)$. Transitions are allowed only between adjacent states $s_m \rightarrow s_m \pm 1$, with s_m understood modulo q.

The spins are driven out of equilibrium by a non-conservative force f > 0, modelled by biasing the dynamics such that it favours counter-clockwise transitions $s_m \rightarrow s_m + 1$ over clockwise transitions $s_m \rightarrow s_m - 1$ [red arrow in Fig. 1(a)]. This way, individual Potts spins rotate on average in direction of the driving and become "Potts oscillators". Potential experimental realisations of driven Potts models are described in the companion paper [19].

The oscillators interact with each other via a global, ferromagnetic potential, that reduces the energy of the system by \mathcal{J}/N whenever two spins are in the same state, see Fig. 1(b).

The stochastic dynamics of the model is determined by transition rates for the transitions $s_m \rightarrow s_m \pm 1$. These rates are constrained by thermodynamic consistency and symmetries, but arbitrary to some degree, which leaves one with free parameters that the model's behaviour depends upon.

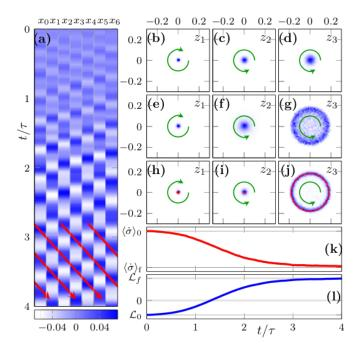


FIG. 2. (a) Synchronisation in real and Fourier space starting from decoherence, using Arrhenius dynamics (details in Ref. [19]) with q = 7, $\beta \mathcal{J}/q = 1.025$, $\beta f = 7$, $N = 10^5$. Arrows indicate evolution in time t in units of the microscopic transition time τ . (a) Deviations x_0, \ldots, x_6 from decoherence. (b)–(j) Probability density of Fourier modes z_1, z_2, z_3 at $t = 0.5\tau$ [(b)–(d)], $t = 2\tau$ [(e)–(g)], and $t = 4\tau$ [(h)–(j)], obtained from an ensemble of 10^3 realisations. Red lines from macroscopic dynamics in Eq. (1). (k) Rate of dissipated work. (l) Phase-space contraction rate.

The state of a large system of Potts oscillators is described by the occupation probability $p(t) = (p_0, ..., p_{q-1})^\mathsf{T}$, $p_n(t)$ denoting the probability of an arbitrary Potts spin s_m to be in state $s_m = n$ at time t. For small $\beta \mathcal{J}$, Potts oscillators rotate decoherently so that p(t) is constant and uniform, $p(t) = p^* \equiv (\frac{1}{q}, ..., \frac{1}{q})^\mathsf{T}$. At a critical value $\beta \mathcal{J}_c$, however, a dynamical phase transition into a synchronised state occurs, in which macroscopic numbers of Potts spins oscillate in synchrony, as observed numerically for $q \le 7$ in Refs. [17, 18]. The synchronised state is a simple example of a dissipative structure that spontaneously breaks time-translation symmetry and exhibits macroscopic order.

Synchronisation is conveniently described by the time-dependent deviations $\mathbf{x}(t) \equiv \mathbf{p}(t) - \mathbf{p}^*$ from decoherence. Figure 2 shows synchronisation in a numerical simulation of a large system of driven Potts oscillators with q = 7. Figure 2(a) shows how initial decoherence $[\mathbf{x}(0) = 0]$ evolves into a synchronisation pattern in $\mathbf{x}(t)$, characterised by three travelling maxima (red arrows).

Discrete rotational symmetry, $s_m = s_m \pm q$, allows to characterise these patterns by discrete complex Fourier modes. As we explain below, there are three dynamical Fourier modes for q = 7, that we denote by z_1, z_2, z_3 with wave numbers k = 1, 2, 3, respectively. The time evolution of these modes in the complex plane is shown in Figs. 2(b)-(j). Initially all

modes are inactive [Figs. 2(b)–(d)], but the amplitudes of the Fourier modes with largest k grow [Figs. 2(e)–(g)]. Eventually [Figs. 2(h)–(j)], only z_3 is active and rotates counter-clockwise in the complex plane (green arrow), reflecting the emergence of the synchronisation pattern shown in Fig. 2(a). By contrast, the amplitudes of z_1 and z_2 are essentially zero.

We employ Stochastic Thermodynamics [13–15] to extract faithful thermodynamic observables from the dynamics. The average rate of dissipated work, shown in Fig. 2(k), is initially large and equal to $\langle \dot{\sigma} \rangle_0$, the average dissipation rate of a single, uncoupled oscillator. During relaxation into the synchronised state, the rate of dissipated work decreases and settles at a smaller value, $\langle \dot{\sigma} \rangle_f$, associated with the average dissipation rate per oscillator in the synchronised phase.

The phase-space contraction rate, shown in Fig. 2(l), is a measure of a state's momentary stability. Its initial value \mathcal{L}_0 is negative, reflecting that decoherent oscillations are unstable, but it increases as function of time, changes sign, and saturates at a positive value $\mathcal{L}_f > 0$, indicating a stable synchronised final state. Comparing Figs. 2(k) and (l) we observe an apparent connection between stability and dissipation.

We explore this connection and derive a stability-dissipation relation, Eq. (18), that links least dissipation and largest stability in a simple way. Our exact derivation is based on the analytic solution of driven Potts models close to the synchronisation transition, discussed in Ref. [19]. Previous relations between stability and dissipation either refer to near-equilibrium situations [1, 2] or lack a coherent thermodynamic interpretation [20–23]. The new relation (18), by contrast, holds far from equilibrium and carries a transparent interpretation, as it rests upon the well-established concepts of Stochastic Thermodynamics [13–15].

On the basis of the dissipation-stability relation, we establish a minimum-dissipation principle [3] for driven Potts models at large but finite N, that holds arbitrarily far from equilibrium, for all dynamics, and for all q. Existing studies of the thermodynamics of synchronisation [24–28] have drawn model-dependent conclusions on whether synchronisation enhances [29, 30] or reduces [17, 31] dissipation. Our results now show that synchronisation reduces dissipation in all driven Potts models, and that the least dissipative non-equilibrium states are dynamically selected close to the phase transition.

MACROSCOPIC DYNAMICS

From a minimal set of requirements, including thermodynamic consistency, symmetry, and a well-defined thermodynamic limit, we show in Ref. [19], that as $N \to \infty$ the occupation probabilities $p_n(t)$ obey the deterministic equations of motion

$$\frac{\mathrm{d}}{\mathrm{d}t}p_n(t) \equiv h_n[\mathbf{p}(t)] = j(p_n, p_{n-1}) - j(p_{n+1}, p_n), \tag{1}$$

n = 0, ..., q - 1, where $j(p_{n+1}, p_n)$ denotes the average probability flux per oscillator from state n to state n + 1. The flux

j is expressed in terms of the rescaled microscopic transition rates w_n^{\pm} for the transitions $s_m \rightarrow s_m \pm 1$, $s_m = n$, as

$$j(p_{n+1}, p_n) = w_n^+(\mathbf{p}) - w_{n+1}^-(\mathbf{p}).$$
 (2)

The LDB condition [13-15] requires that

$$\frac{w_n^{\pm}(\boldsymbol{p})}{w_{n+1}^{\mp}(\boldsymbol{p})} = \exp\left\{-\beta\left[(\partial_{p_{n\pm 1}} - \partial_{p_n})\mathcal{F}(\boldsymbol{p}) \mp f\right]\right\}, \quad (3)$$

where f denotes the non-conservative force and

$$\mathcal{F}(\boldsymbol{p}) = -\frac{\mathscr{J}}{2} \boldsymbol{p} \cdot \boldsymbol{p} + \beta^{-1} \boldsymbol{p} \cdot \log \boldsymbol{p}, \qquad (4)$$

denotes the free energy per oscillator.

From Eq. (1), we immediately find that the decoherent state p^* is a fixed point with $\frac{d}{dt}p|_{p=p^*}=0$. A linear stability analysis reveals that the stability of p^* depends on the sign of the bifurcation parameter [19]

$$\Lambda = 2(j_{10} - j_{01}), \tag{5}$$

where we denote by j_{nm} the derivatives of the probability flux j at the decoherent fixed point:

$$j_{nm} \equiv \partial_y^n \partial_x^m j(y, x)|_{x=y=\frac{1}{a}}.$$
 (6)

The fixed point p^* is stable for $\Lambda < 0$ and unstable for $\Lambda > 0$, so that perturbations of decoherence grow, whenever Λ is positive.

The location in parameter space where Λ changes sign depends on the transition rates. Figure 3(a) shows the phase boundaries ($\Lambda = 0$) for different w_n^{\pm} . In the equilibrium limit $\beta f \to 0$, all phase boundaries approach $\beta \mathcal{J}_c/q = 1$ [32]. Away from equilibrium, for $\beta f > 0$, varying w_n^{\pm} may either stabilise the decoherent phase (blue arrow), destabilise it (red arrow), or retain the phase boundary of the equilibrium case (solid line), see Ref. [19] for examples.

For $\Lambda > 0$, when the decoherent fixed point is unstable, fluctuations drive the system away from decoherence and towards other attractive states. Such states can be either distant attractors such as ordered states, as is the case at equilibrium [32] and for weak driving [17], or nearby, small-amplitude variations of p^* . Candidates for the latter are coherent oscillations (synchronisation) and stationary, non-equilibrium patterns.

ANALYTIC SOLUTION

In order to explore the possible stable structures in the vicinity of the decoherent fixed point p^* , we solve the driven Potts model exactly for small x. To this end, we exploit the periodicity of Potts spins and transform the variation vector x into discrete Fourier modes \hat{x} by means of a Fourier transform $\hat{x} = \mathbb{F}x$, where \mathbb{F} is a $q \times q$ matrix with elements $F_{kn} = \exp(i2\pi kn/q)$, $k = 0, \dots, q-1$. The inverse transform \mathbb{F}^{-1} is obtained by Hermitian conjugation: $\mathbb{F}^{-1} = q^{-1}\mathbb{F}^{\dagger}$.

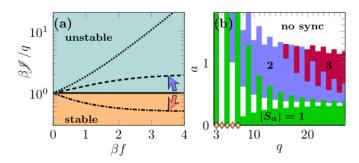


FIG. 3. (a) Stability of decoherent phase in the βf - $\beta \mathcal{J}/q$ plane with phase boundaries for different dynamics (broken and solid lines, details in Ref. [19]). (b) Phase diagram of small-amplitude synchronised states in driven Potts models as function of q and a [Eq. (14)]. Numbers indicate how many Fourier modes are active. Markers show the parameters of previous numerical studies [17, 18].

This way, we obtain the equation of motion for \hat{x} :

$$\hat{\mathbf{x}} \equiv \hat{\mathbf{h}}(\hat{\mathbf{x}}), \qquad \hat{\mathbf{h}}(\hat{\mathbf{x}}) \equiv \mathbb{F}\mathbf{h}(\mathbb{F}^{-1}\hat{\mathbf{x}} + \mathbf{p}^*).$$
(7)

In the vicinity of the decoherent fixed point, $|\hat{\mathbf{x}}| \ll 1$, we expand $\hat{\mathbf{h}}(\hat{\mathbf{x}})$ to third order in $\hat{\mathbf{x}}$, i.e.,

$$\hat{h}(\hat{x}) \sim \hat{h}^{(1)}(\hat{x}) + \hat{h}^{(2)}(\hat{x}) + \hat{h}^{(3)}(\hat{x}),$$
 (8)

where $\hat{\boldsymbol{h}}^{(n)}$, n = 1, ..., 3, are n^{th} -order polynomials in $\hat{\boldsymbol{x}}$.

The linear part $\hat{h}^{(1)} = \mathbb{D}\hat{x}$ contains the stability matrix \mathbb{D} , diagonal in the Fourier basis, with elements $\mathbb{D}_{kk} = \mu_k + i\omega_k$ and

$$\mu_k = \Lambda \sin^2\left(\frac{\pi k}{q}\right), \quad \omega_k = \Omega \sin\left(\frac{2\pi k}{q}\right).$$
 (9)

The imaginary part ω_k of \mathbb{D}_{kk} , with parameter

$$\Omega = j_{10} + j_{01} = q j_{00} \,, \tag{10}$$

denotes the "natural frequency" of the $k^{\rm th}$ Fourier mode, with which the dynamics spirals away from p^* for $\Lambda > 0$ [19].

Where the dynamics takes $\hat{x}(t)$ in the long-time limit depends on the higher-order terms in Eq. (8). Before we consider these, we note that x is real, so that the Fourier modes \hat{x} are related by complex conjugation. We define

$$z_k \equiv \hat{x}_k \,, \qquad \bar{z}_k \equiv \hat{x}_{-k} \,, \tag{11}$$

with $k = 1, ..., \lfloor \frac{q}{2} \rfloor$ (indices modulo q). The zeroth mode $z_0 = \hat{x}_0$ vanishes due to probability conservation, leaving the driven q-state Potts model with $\lfloor \frac{q}{2} \rfloor$ dynamic Fourier modes, as stated for q = 7 in the Introduction.

The non-linear terms in Eq. (8) are brought into the simpler normal form [19]

$$\dot{z}_{k}^{\prime} \sim \left(\mathbb{D}_{kk} - \sum_{k=1}^{\lfloor \frac{q}{2} \rfloor} \mathbb{C}_{kk^{\prime}} |z_{k^{\prime}}^{\prime}|^{2} \right) z_{k}^{\prime}, \tag{12}$$

by a non-linear transformation $z_k \mapsto z_k'$, where \mathbb{C} is a complex matrix. The normal form (12) retains only terms that are essential for the transition when $0 < \Lambda \ll 1$ and $\Lambda \ll \beta f$ [33].

To determine the long-time states, we separate the Fourier modes z_k' into their amplitudes r_k and phases ϕ_k , $z_k' = r_k \exp(i\phi_k)$. The normal form (12) then decomposes into a phase equation for ϕ and an amplitude equation for r. The latter reads

$$\dot{r}_k \sim \left(\mu_k - \sum_{k'=1}^{\lfloor \frac{q}{2} \rfloor} \mathbb{A}_{kk'} r_{k'}^2\right) r_k$$
 (13a)

with [19]

$$\mathbb{A} \equiv \operatorname{Re}(\mathbb{C}) = A\left(\boldsymbol{u}\boldsymbol{v}^{\mathsf{T}} - \mathbb{W}\right), \quad A \equiv \frac{4}{q^2}(j_{03} - j_{30}), \quad (13b)$$

and contains the essential parameters for r close to the transition. The vectors u, v and the diagonal matrix \mathbb{W} depend only on the single parameter

$$a = \frac{j_{02}^2 - j_{20}^2}{q j_{00}(j_{03} - j_{30})} - 1.$$
 (14)

Both stable synchronised states and stationary patterns with $\dot{\phi} = 0$ are given by the stable fixed points r^* of Eq. (13a), i.e., $\dot{r}|_{r=r^*} = 0$. Because of the simple structure (13b) of \mathbb{A} , these fixed points can be obtained explicitly [19].

Following this program, we arrive at the phase diagram of small-amplitude synchronised states in the q-a parameter space, given in Fig. 3(b). In the white regions, no synchronised states are stable. Different colours indicate stable synchronisation patterns with a finite number $|S_a|$ of nonvanishing, i.e. active, Fourier modes. The amplitudes of the remaining $\lfloor \frac{q}{2} \rfloor - |S_a|$ modes vanish, i.e. these modes are inactive.

The green region ($|S_a| = 1$) exhibits multistability, i.e., several synchronised states, each with a different active mode, are simultaneously stable [19]. The other coloured regions with $|S_a| > 1$ host unique stable synchronised states.

The white patches between the green and blue regions in Fig. 3(b) occur only for even q. Although they host no synchronised states, they admit stationary probability patterns [19]. Note that previous numerical studies [17, 18], shown as markers in Fig. 3(b), covered only a tiny fraction of the parameter space.

STABILITY-DISSIPATION RELATION

We now derive the main result of this Letter, a stability-dissipation relation, that holds for all dynamics that admit stable small-amplitude states, including both synchronisation and stationary patterns. To this end, we introduce the average entropy production rate $\langle \dot{\sigma} \rangle$ per oscillator [34], which for $N \to \infty$ takes the form [19]

$$\langle \dot{\sigma} \rangle = \sum_{n=0}^{q-1} F(p_{n+1}, p_n) j(p_{n+1}, p_n),$$
 (15)

where $F(p_{n+1}, p_n) = \beta \left[f - (\partial_{p_{n+1}} - \partial_{p_n}) \mathcal{F}(\mathbf{p}) \right]$ are thermodynamic forces that drive the fluxes $j(p_{n+1}, p_n)$.

We define the change in entropy production $\Delta \dot{\sigma}$ relative to the entropy production rate of a single Potts oscillator $\langle \dot{\sigma} \rangle_0 = 2\beta f \sinh(\beta f/2)$ [17, 18] by $\Delta \dot{\sigma} = (\langle \dot{\sigma} \rangle - \langle \dot{\sigma} \rangle_0)/|\langle \dot{\sigma} \rangle_0|$, express $\langle \dot{\sigma} \rangle$ in terms of Fourier modes, and expand around the decoherent fixed point $\hat{x} = 0$. Exploiting the symmetries of driven Potts models and the general properties of the transition rates, we obtain the simple expression [19]:

$$\Delta \dot{\sigma} \sim -2\Gamma \lambda \alpha_a < 0, \qquad \Gamma \equiv \frac{2j_{11}}{q^2 j_{00}}, \qquad (16)$$

valid for $0 < \Lambda \ll 1$ and $\Lambda \ll \beta f$ [33]. The parameters $\lambda \equiv \Lambda/A$ and $\Gamma > 0$ are dynamics dependent, while $\alpha_a > 0$ depends on the set of active Fourier modes in a given stable state and on a [19]. Equation (16) shows that entropy production is reduced in any stable small-amplitude state.

Finally, we connect $\Delta \dot{\sigma}$ to the stability change across the transition. To this end, we consider the average $\langle L \rangle$ of the stochastic inflow rate L [35], the difference between the entrance rate, the sum of all transition rates of adjacent states entering a given state, and the escape rate out of this state.

In the thermodynamic limit, $\langle L \rangle$ converges to the phase-space contraction rate \mathcal{L} , i.e., $\lim_{N\to\infty}\langle L \rangle = \mathcal{L}$ [19], given by $\mathcal{L} = -\nabla_{\boldsymbol{p}} \cdot \dot{\boldsymbol{p}}$ [36]. Phase-space probability accumulates in regions of positive \mathcal{L} , while it escapes regions of negative \mathcal{L} . Positive \mathcal{L} is a necessary condition for fixed points and periodic orbits to be approached in the long-time limit.

We analyse the relative stability change $\Delta \mathcal{L} = (\mathcal{L} - \mathcal{L}_0)/|\mathcal{L}_0|$ of \mathcal{L} close to the transition, where $\mathcal{L}_0 \equiv -q\Lambda/2$ denotes the phase-space contraction rate at p^* . Expanding $\Delta \mathcal{L}$ around $\hat{\mathbf{x}} = 0$, we find [19]

$$\Delta \mathcal{L} \sim 2\alpha_a > 0, \tag{17}$$

implying that small-amplitude states are more stable (\mathcal{L} is larger) than p^* for $\Lambda > 0$.

Combining Eq. (17) with Eq. (16), we arrive at the stability-dissipation relation

$$\Delta \dot{\sigma} \sim -\Gamma \lambda \Delta \mathcal{L}$$
, (18)

the main results of this Letter. It shows that, close to the transition, $\Delta \dot{\sigma}$ depends linearly on $\Delta \mathcal{L}$ with negative, dynamics-dependent prefactor $-\Gamma \lambda$, so that dissipation is smallest in the most stable small-amplitude state.

We have tested the stability-dissipation relation numerically, using both the macroscopic (1) and the stochastic dynamics. The latter involves an additional long-time average [19]. Figure 4 shows $\Delta \dot{\sigma}$ plotted against $\lambda \Delta \mathcal{L}$ for two different sets of transition rates with $(a,\Gamma)=(0,1/2)$ and $(a,\Gamma)=(1,1)$ [19]. For values of $\Delta \dot{\sigma}$ and $\lambda \Delta \mathcal{L}$ close to the transition, the simulations confirm Eq. (18).

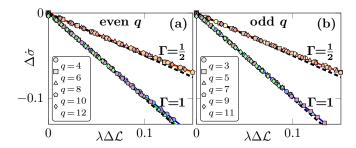


FIG. 4. Stability-dissipation relation for two different dynamics with $N = 10^6$ and $\beta f = 7$, obtained from a time average with $t/\tau \approx 100$. (a) Even q. Markers from numerical simulations of the stochastic dynamics, solid lines from the macroscopic dynamics (1). The dashed line shows Eq. (18). (b) Same as in (a) but for odd q.

MINIMUM-DISSIPATION PRINCIPLE

Finally, we establish the minimum-dissipation principle for driven Potts models. When the thermodynamic limit is taken before a long-time limit, Eq. (18) alone does not directly imply such a principle, because the infinite-size system is in general non-ergodic and the most stable states are assumed only if the initial condition lies in their basins of attraction. However, when long times are invoked first, fluctuations enable frequent transitions between different states that are sufficiently close. This holds for $\lambda \ll 1$, where all small-amplitude states and the decoherent state are separated only by small distances of order $\sqrt{\lambda}$, while finite-size fluctuations are of order $1/\sqrt{\mathcal{L}N/q} \ll 1/\sqrt{\lambda N}$. Hence, stable small-amplitude states are frequently visited when $1 \ll N \lesssim \lambda^{-2}$.

In this case, the system predominantly occupies stable states with largest $\langle L \rangle$, because once a (stochastic) trajectory has reached such a state, it typically spends a long time there, compared to the average entrance time. Equation (18) then implies that driven Potts models probabilistically select small-amplitude states with largest $\langle L(N) \rangle \to \mathcal{L}$ and thus smallest dissipation [37]. In numerical simulations, we find that the minimum-dissipation principle holds for substantially larger N and λ than our argument suggests [19], which is why $1 \ll N \lesssim \lambda^{-2}$ should be considered a conservative estimate.

CONCLUSION

We have proved a linear stability-dissipation relation (18) for driven Potts models, which shows that the most stable dissipative structures dissipate the least entropy. For large but finite systems, we argued that Eq. (18) implies a minimum-dissipation principle for driven Potts models, that holds arbitrarily far away from equilibrium, independently of the dynamics, and for all q. The dissipation and stability measures $\dot{\sigma}$ and L can be defined for any thermodynamically consistent stochastic system. We are therefore confident that the tools developed here will facilitate further connections between non-equilibrium thermodynamics and stability. For instance, pre-

liminary results suggest a relation similar to Eq. (18) for Potts oscillators with local interactions.

ACKNOWLEDGMENTS

We thank G. Falasco for insightful discussions and for pointing out the notion of phase-space contraction in stochastic systems. J.M.'s stay at King's College London was supported by a Feodor-Lynen scholarship of the Alexander von Humboldt-Foundation and M.E. by the ChemComplex project (C21/MS/16356329) funded by FNR (Luxembourg).

- [1] Ilya Prigogine and Paul Glansdorff, *Thermodynamic Theory* of *Structure*, *Stability and Fluctuations* (Wiley-Interscience, 1971)
- [2] Dilip Kondepudi and Ilya Prigogine, Modern thermodynamics: From Heat Engines to Dissipative Structures (Wiley, New York, 2014).
- [3] Ilya Prigogine, *Introduction to Thermodynamics of Irreversible Processes* (Charles C Thomas, Springfield, IL, 1955).
- [4] Jürgen Schnakenberg, "Network theory of microscopic and macroscopic behavior of master equation systems," Reviews of Modern Physics 48, 571 (1976).
- [5] Chung Yuan Mou, Jiu-li Luo, and Gregoire Nicolis, "Stochastic thermodynamics of nonequilibrium steady states in chemical reaction systems," The Journal of Chemical Physics 84, 7011– 7017 (1986).
- [6] Danilo Forastiere, Riccardo Rao, and Massimiliano Esposito, "Linear stochastic thermodynamics," New Journal of Physics 24, 83021 (2022).
- [7] Danilo Forastiere, Francesco Avanzini, and Massimiliano Esposito, "Dissipation in Hydrodynamics from Micro-to Macroscale: Wisdom from Boltzmann and Stochastic Thermodynamics," New Journal of Physics 26, 063022 (2023).
- [8] Luo Jiu-Li, Christian van den Broeck, and Grégoire Nicolis, "Stability criteria and fluctuations around nonequilibrium states," Zeitschrift für Physik B Condensed Matter 56, 165–170 (1984).
- [9] Grégoire Nicolis, "Thermodynamic theory of stability, structure and fluctuations," Pure and Applied Chemistry 22, 379– 392 (1970).
- [10] Rolf Landauer, "Inadequacy of entropy and entropy derivatives in characterizing the steady state," Physical Review A 12, 636 (1975).
- [11] Edwin T Jaynes, "The minimum entropy production principle," Annual Review of Physical Chemistry **31**, 579–601 (1980).
- [12] G Kirchhoff, "Ueber die Anwendbarkeit der Formeln für die Intensitäten der galvanischen Ströme in einem Systeme linearer Leiter auf Systeme, die zum Theil aus nicht linearen Leitern bestehen," Annalen der Physik 151, 189–205 (1848).
- [13] Udo Seifert, "Stochastic thermodynamics, fluctuation theorems and molecular machines," Reports on Progress in Physics 75, 126001 (2012).
- [14] Christian den Broeck and Massimiliano Esposito, "Ensemble and trajectory thermodynamics: A brief introduction," Physica A: Statistical Mechanics and its Applications 418, 6–16 (2015).
- [15] Luca Peliti and Simone Pigolotti, *Stochastic Thermodynamics: An Introduction* (Princeton University Press, Princeton, NJ,

- 2021).
- [16] Gianmaria Falasco and Massimiliano Esposito, "Macroscopic stochastic thermodynamics," Review of Modern Physics 97, 015002 (2025).
- [17] Tim Herpich, Juzar Thingna, and Massimiliano Esposito, "Collective power: Minimal model for thermodynamics of nonequilibrium phase transitions," Physical Review X 8, 031056 (2018).
- [18] Tim Herpich and Massimiliano Esposito, "Universality in driven Potts models," Physical Review E 99, 022135 (2019).
- [19] Jan Meibohm and Massimiliano Esposito, "Small-amplitude coherent oscillations in driven Potts models," Physical Review E 110, 044114 (2024).
- [20] David Ruelle, "Positivity of entropy production in nonequilibrium statistical mechanics," Journal of Statistical Physics 85, 1–23 (1996).
- [21] David Daems and Grégoire Nicolis, "Entropy production and phase space volume contraction," Physical Review E 59, 4000 (1999).
- [22] Debra J Searles and Denis J Evans, "The fluctuation theorem and Green–Kubo relations," The Journal of Chemical Physics 112, 9727–9735 (2000).
- [23] Denis J Evans and Gary P Morriss, Statistical Mechanics of Nonequilbrium Liquids (ANU Press, Canberra, ACT, 2007).
- [24] Alberto Imparato, "Stochastic thermodynamics in many-particle systems," New Journal of Physics 17, 125004 (2015).
- [25] Shin-ichi Sasa, "Collective dynamics from stochastic thermodynamics," New Journal of Physics 17, 45024 (2015).
- [26] Pedro D Pinto, Andre L A Penna, and Fernando A Oliveira, "Critical behavior of noise-induced phase synchronization," Europhysics Letters 117, 50009 (2017).
- [27] Marc Suñé and Alberto Imparato, "Out-of-equilibrium clock model at the verge of criticality," Physical Review Letters 123, 070601 (2019).

- [28] Michalis Chatzittofi, Ramin Golestanian, and Jaime Agudo-Canalejo, "Collective synchronization of dissipatively-coupled noise-activated processes," New Journal of Physics 25, 093014 (2023).
- [29] Dongliang Zhang, Yuansheng Cao, Qi Ouyang, and Yuhai Tu, "The energy cost and optimal design for synchronization of coupled molecular oscillators," Nature physics 16, 95–100 (2020).
- [30] Laura Guislain and Eric Bertin, "Discontinuous phase transition from ferromagnetic to oscillating states in a nonequilibrium mean-field spin model," Physical Review E 109, 034131 (2024).
- [31] Yuki Izumida, Hiroshi Kori, and Udo Seifert, "Energetics of synchronization in coupled oscillators rotating on circular trajectories," Physical Review E 94, 052221 (2016).
- [32] Fa-Yueh Wu, "The Potts model," Reviews of Modern Physics **54**, 235 (1982).
- [33] These limits should be understood as conservative mathematical statements. We find numerically that Eqs. (12), (16), and (17) hold also for moderate Λ and βf .
- [34] We express all entropy measures in dimensionless form, i.e., in units of $k_{\rm B}$.
- [35] Marco Baiesi and Gianmaria Falasco, "Inflow rate, a timesymmetric observable obeying fluctuation relations," Physical Review E 92, 042162 (2015).
- [36] Edward Ott, Chaos in Dynamical Systems (Cambridge University Press, Cambridge, U.K., 2002).
- [37] See Ref. [19] and the Supplemental Material [38] for numerical confirmations at q = 9 and q = 17.
- [38] See Supplemental Material at http://link.aps.org/ supplemental/10.1103/PhysRevE.110.L042102 for videos that illustrate the minimum-dissipation principle..